Novel Thermal Barrier Coatings with Hexagonal Boron Nitride Additives Resistant to Molten Volcanic Ash Wetting

Siddharth Lokachari [a], Wenjia Song [a,*], Masahiro Fukumoto [c], Yan Lavallée [d], Hongbo Guo [e], Yancheng You [b,*], Donald B. Dingwell [a]

[a] Department of Earth and Environmental Sciences, Ludwig Maximilians Universität München, Theresienstrasse 41, 80333 Munich, Germany

[b] School of Aerospace Engineering, Xiamen University, 361102 Xiamen, China

[c] Department of Mechanical Engineering, Toyohashi University of Technology, 1-1 Tempaku-cho, 441-8580 Toyohashi, Japan

[d] Department of Earth, Ocean and Ecological Sciences, University of Liverpool, Liverpool L69 3GP, UK

[e] School of Materials Science and Engineering, Beihang University, 100191 Beijing, China

***Corresponding authors**:

Wenjia Song, Department of Earth and Environmental Sciences, Ludwig-Maximilians-Universität (LMU), Theresienstrasse 41, 80333 Munich, Germany. (wenjia.song@lmu.de)
Telephone: +49 (0) 89 2180 4293

Yancheng You, School of Aerospace Engineering, Xiamen University, 361102 Xiamen, China. (yancheng.you@xmu.edu.cn)

Telephone: +86 (0) 592 2186 849

Abstract

Yttria-stabilized zirconia thermal barrier coatings (YSZ TBCs) are prone to degradation by atmospheric contaminants such as volcanic ash, posing a serious threat to their durability. Here we demonstrate that hexagonal boron nitride (*h*-BN) additives to YSZ coatings (*h*-BN YSZ), exhibit resistance against volcanic ash interaction at 1250 °C. In preliminary tests performed under vacuum, *h*-BN YSZ coatings demonstrate greatly inhibited wetting against molten volcanic ash drops. Under oxidizing conditions, *h*-BN YSZ provide enhanced wetting and chemical resistance over conventional coatings. This study lays groundwork for the development of novel additives which are physico-chemically resilient against molten volcanic ash wetting.

Keywords: Thermal Barrier Coatings, Hexagonal Boron Nitride, Volcanic ash, Non-wetting, Silica-phobicity.

1. Introduction

With the steady growth of global air traffic, the occurrence rate of volcanic ash plume encounters by aircrafts has soared and the hazards generated by the ingestion of molten silicate deposits into the engines have garnered greater attention leading to deeper investigation in the aviation sector [1–7]. In 2010, the eruption of Eyjafjallajökull in Iceland triggered the largest aviation shutdown in Europe since World War II and caused economic losses estimated at ~2 billion euros [8,9]. Given the catalytic role of air travel in shaping socio-economic forces across the globe, diminishing the potential impact of environmental dust in general, molten calcium magnesium alumino-silicate (CMAS) deposits and volcanic ash in particular on aviation safety has become a research and development imperative [10,11].

When volcanic ash is ingested into a modern jet engine, it may initially erode/abrade compressor blades, leading to a reduction in operational efficiency, the ash subsequently enters the combustion chamber where peak flame temperatures can reach 2000 ºC [12]. Such temperatures far exceed the melting temperatures (~900 ºC–1300 ºC) of the glassy and mineral constituents of volcanic ash [13,14]. As a result, the ingested ash particles liquify (by glass softening and/or mineral melting) and may adhere to, and flow across (i.e., impaction, spreading and wetting) the surfaces of the engine components (e.g., nozzle guide vanes and high-pressure turbine blades) that are commonly protected by thermal barrier coatings (TBCs) [15–18].

Conventional TBCs are porous ceramic coatings (typically made of tetragonal-phase ZrO_2 ceramic stabilized by 6–8 wt.% Y_2O_3, commonly referred to as YSZ) prepared by atmospheric plasma-spraying (APS) or electron-beam physical vapor deposition (EB-PVD) [19, 20]. Molten volcanic ash can rapidly ingress into the porous coating due to capillary action, thereby cause spallation of the TBCs due to stiffening as a resultant of infiltrated melt solidification during cooling [21]. Simultaneously, a chemical interaction takes place between molten volcanic ash and YSZ coating consisting of the dissolution of initial metastable tetragonal (t') YSZ grains in the molten CMAS followed by precipitation of Y depleted m-ZrO_2 [22]. In the past ten years, it has been suggested that the most promising solution for mitigation of the infiltration of molten volcanic ash into TBCs might be achieved by Gadolinium zirconate TBCs ($Gd_2Zr_2O_7$) [23, 24]. $Gd_2Zr_2O_7$ TBCs counteract silicate melt infiltration thermo-chemically by crystallizing the melt and

formation of oxy-apatite phase upon reaction [25]. The inclusion However, the deterioration of TBC primarily emanates due to wetting of molten volcanic ash on the surface [18]. To expand the scope of potential mitigational measures to counteract molten volcanic ash wetting, we go beyond the state of art of traditional TBC materials. Here, we introduce the design of a more resilient *h*-BN additives to YSZ with properties that reduce silicate melt wettability, and thereby inhibit physical infiltration and degradation via chemical reaction.

2. Experimental Procedure

2.1 Fresh volcanic ash characterization and homogenization

(a)

Elements	SiO_2	Al_2O_3	MgO	MnO	Na_2O	CaO	FeO	TiO_2	K_2O
Eyjafjallajökull (wt. %)	59.70	15.72	2.41	0.23	5.61	4.55	8.01	1.39	2.30
Santa Maria (wt. %)	62.15	19.64	1.41	0.12	4.49	5.99	3.99	0.51	1.46
Soufriere Hills (wt. %)	65.74	16.00	2.12	0.14	3.38	5.57	5.28	0.51	1.06

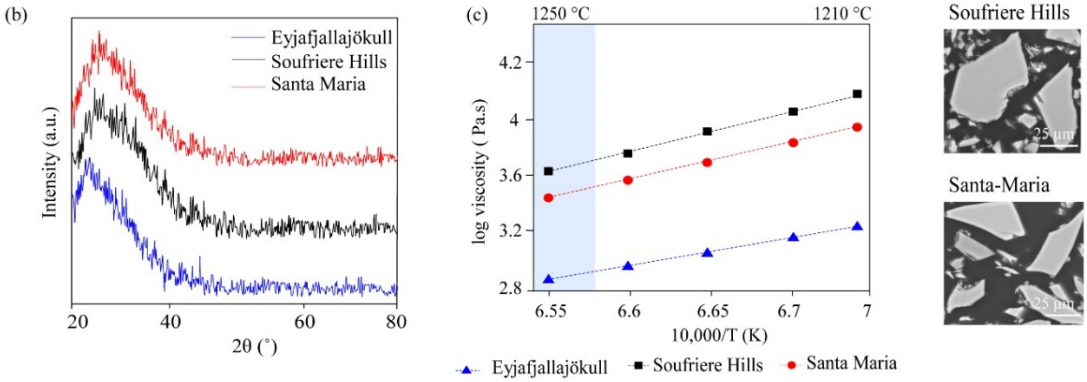

Fig. 1. Characterization of volcanic ashes. (a) Bulk chemical composition of volcanic ashes. (b) XRD spectra of the re-melted volcanic ashes showing only the amorphous silica shoulder, further confirming the amorphous character of the ash samples. (c) Viscosity of the ash samples over the temperature range 1210 °C–1250 °C. (d) SEM images of re-melted Eyja, SF and SM ashes.

Three fresh volcanic ash samples were utilized for this experiment: Eyjafjallajökull (Eyja), Soufriere Hills (SH), and Santa Maria (SM). Bulk chemical composition of the volcanic ashes was determined by X-ray fluorescence spectrometry (XRF) (Fig. 1a). The crystal-bearing natural volcanic ash samples were heated in a platinum crucible to 1650 °C for 48 hours and were subsequently quenched in air, to produce crystal-free glasses with a common thermal history. The glasses were then crushed and sieved to produce finely

powdered ash. X-ray diffraction (XRD) pattern was measured for the glassy samples of the re-melted ash (GE X-ray diffractometer 3003 TT) (Fig. 1b).

The viscosity of the molten volcanic ash as a function of temperature was estimated using multi-component viscosity evaluation model, developed by Giordano *et.al* [26] (Fig. 1c). The re-melted volcanic ash samples were optically investigated using a scanning electron microscope (SEM) (Fig. 1d). SEM and XRD results confirmed that the ash samples were homogeneous. The onset of melting was estimated using the rhyolite-MELTS software (Onset of melting: Eyja: 1151 °C, SM: 1179 °C, SH: 1130 °C) [27].

2.2 Fabrication of the TBCs

We employed APS method to produce novel coatings consisting of *h*-BN (20 wt.%) and 7YSZ (80 wt.%) (referred to as *h*-BN YSZ) onto an alumina substrate (Al_2O_3 > 96%). 7 wt. %YSZ powder with a particle size of less than 63 µm (Fujimi) and boron nitride powder with a particle size of less than 45 µm (Alfa Aesar) were used as feedstock. Alumina substrates were chosen in this work instead of traditional superalloy substrates to facilitate isothermal heat treatment of the system above 1200 °C. Conventional YSZ coatings were fabricated by thermal spraying (Table 1), for comparative tests *versus h*-BN YSZs with same spray conditions (referred to as YSZ). The coatings were ultrasonically cleaned using de-ionized water post fabrication, and stored in a desiccator in order to avoid any surficial contamination.

Table 1. Plasma spray parameters.

Arc Voltage (V)	Carrier gas (Ar- L·min^{-1})	Arc current (A)	Spray distance (mm)	Powder feed rate (g·min^{-1})
70	40	800	100	0.8

2.3 Wettability measurement and Thermal aging experiments

The volcanic ash was compacted into cylindrical pellets with radius and height of 1 mm by pressing the ash into a cylindrical die. The resulting cylindrical ash compact was ejected from the die onto the TBC substrate. Wettability was assessed using sessile drop method by monitoring silhouette transition of the ash compact in a Dataphysics OCA 25-HTV 1800 optical dilatometer, at a temperature of 1250 °C, with a heating rate 5 °C min^{-1} and a hold duration of 1 hour. The experiments were performed in atmospheric conditions and

under vacuum conditions, the latter using a turbomolecular pump (< 10^{-5} Pa). The images were captured at 60 frames per second (fps), using a charge coupled device. The contact angle was determined to quantify the wettability of molten volcanic ash on TBCs, from the binary converted real time pictures of the molten drop at 1250 °C. A localized methodology of enclosing the contours of the binary drop allows us to evaluate the equilibrium contact angle-θ_c based on enclosed B-spline, using the drop snake plugin in image J software [28]. The extent of spreading of molten volcanic ash on the coatings post thermal aging was evaluated by the spreading area. Thermal aging process was performed using EM301 Hesse instruments furnace. Ash pellets with radius and height of 1 mm were loaded onto the geometrical centre of the coatings, and they were thermally aged at 1250 °C with a heating rate of 10 ºC min^{-1} for a soak-time of 3–48 hrs and cooled at 10 ºC min^{-1}.

2.4 Micro-hardness measurement

The microhardness of the coatings was measured using Vickers micro-indentation technique (Wilsson VH-1202). The coatings were sectioned across the cross-section and standard metallographic techniques were employed to polish the samples, for Vickers indentation and characterization of the infiltration depth of molten volcanic ash into the coatings. 6 micro-indents were placed across the cross-section of the coatings, at different depths (50, 75, 100 and 150 µm), with a load of 300 gmf. and a hold-time of 10 seconds. The Vickers micro-hardness (H_v) was evaluated by using the following equation:

$$H_v = 0 \cdot 102\frac{F}{S}$$

where F is the indentation load (N) and S is the indented surface area (mm^2).

2.5 Characterization Procedures

Standard metallographic techniques were employed to polish the samples and observe the cross-section. Surface roughness (R_a) of the coatings was evaluated using a Keyence VK-X1000 3D-laser scanning microscope. Raman spectroscopic analysis was performed using a (Horiba Xplora) system, with a wavelength of 532 nm. The samples were subsequently investigated by SEM and energy dispersive

spectroscopic (EDS) analysis to measure the maximum infiltration depth. The average porosity was estimated across the cross section of infiltrated samples by utilizing ImageJ software.

3. Results and Discussion

3.1 TBC Characterization

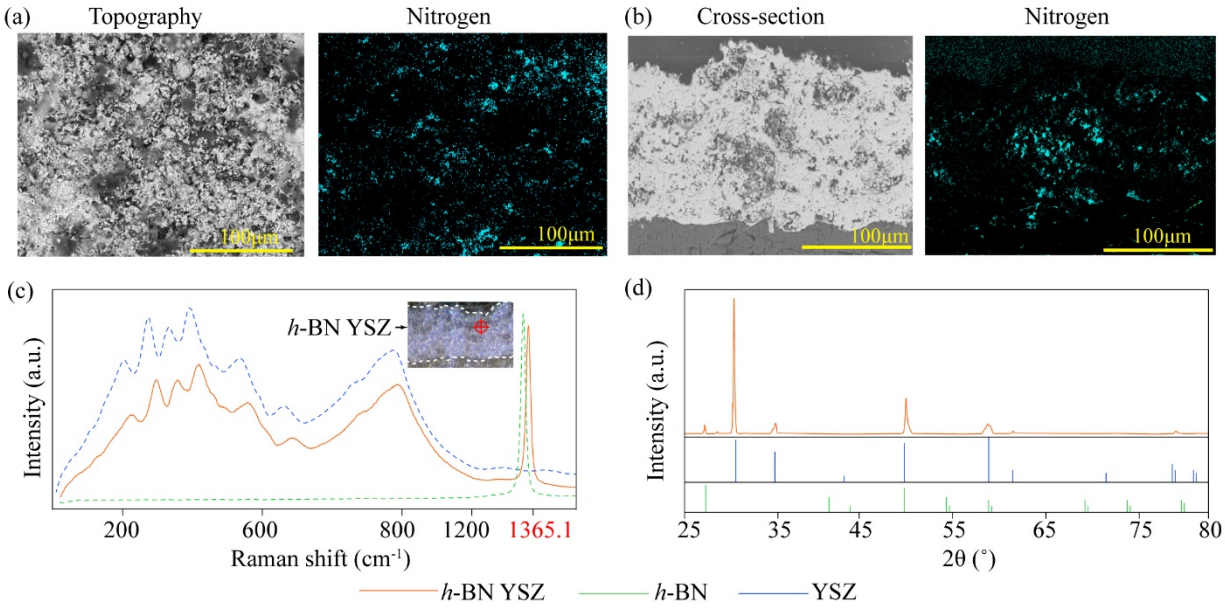

Fig. 2. Characterization of *h*-BN YSZ. (a) SEM image of *h*-BN YSZ coating surface and the corresponding distribution of nitrogen obtained by EDS. (b) Cross-sectional SEM image of *h*-BN YSZ coating and the corresponding nitrogen distribution obtained by EDS. (c) Raman spectra acquired at the cross-section of YSZ, *h*-BN YSZ coating and cross-section of *h*-BN substrate. (d) X-ray diffraction pattern of the *h*-BN YSZ TBC indicates the presence of *h*-BN and *t*-YSZ, as compared to standard *h*-BN (crystallography open database (COD): 2016170) and *t*-YSZ (COD: 1521477) XRD profile data.

As-sprayed YSZ and *h*-BN YSZ coatings consist of a lamellar structure formed by coarse splat like microstructure. The average porosity of *h*-BN YSZ is ~29% , which is slightly higher than that of YSZ coatings (~22 %) . Surface roughness (R_a) values of *h*-BN YSZ and YSZ coatings are 7.3 ± 1.02 µm and 6.8 ± 0.18 µm, respectively (See Fig. S1). R_a of TBCs play an important role in the wetting of molten volcanic ash and it was ensured that R_a was uniform across the surface (Fig. S2). The quality of the *h*-BN additives in the *h*-BN YSZ coatings might be compromised by oxidization in air at high temperatures (~1100°C) [29]. Thus, particular attention was paid to characterizing any potential oxidation. Coating mapping using electron dispersive spectroscopy identified a small fraction of nitrogen (N), scattered onto and within the coating, suggesting minor oxidation (Figs. 2a and 2b). Raman spectral mapping of the coating revealed a

peak at 1365 cm^{-1} (Fig. 2c) and XRD providing unambiguous evidence for the presence of pure (non-oxidized) *h*-BN particulates in the coating. XRD of the coating further indicates the presence of both *h*-BN (peak: 27°) and tetragonal YSZ (*t*-YSZ) (peak range: 34.6–35.8°), as expected in a well fabricated *h*-BN YSZ TBC (Fig. 2d). *Hence, we must conclude that the oxidation of h-BN in the coating remains minor during our experiments.*

3.2 Wetting resistance of *h*-BN YSZ against molten volcanic ash

Hexagonal boron nitride (*h*-BN) is currently regarded (to best of our knowledge) as the sole refractory ceramic material exhibiting a non-wettability of molten Si inferred to be due to its covalently-bonded structure, involving honeycomb-structured sheets bound by weak ionic inter-planar attractions [30–32]. To evaluate the wettability of *h*-BN with molten volcanic ash, a single Eyja glass shard was loaded onto *h*-BN substrate (Fig. 3a) and the sample assembly was heated to 1250 °C (Figs. 3b and 3c). Once cooled to ambient room temperature, it was observed that solidified Eyja glass exhibited non-wetting and non-sticking properties on *h*-BN substrate (Fig. 3d and Movie S1). The non-wetting of molten Eyja ash on the h-BN substrate could be attributed to surficial reaction process, by the formation of Si_3N_4 layer [33].

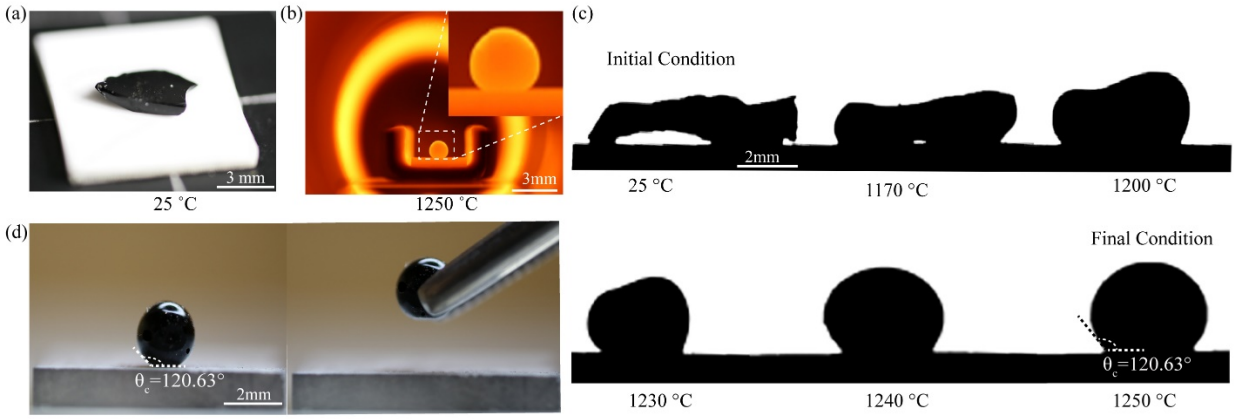

Fig. 3. Non-wetting behavior of hexagonal-boron nitride (*h*-BN) thin film substrate. (a) Eyja glass shard before thermal treatment on *h*-BN thin film substrate. (b) Real time photograph of the molten Eyja at 1250 °C, in-vacuo condition. (c) Sequential In-situ silhouette morphological transition of the irregular shard to a sphere from 25 °C to 1250 °C. (d) Photographs showing the non-wetting behavior (left) and non-adhesion property (right) of solidified melt on the surface of *h*-BN substrate.

To evaluate the wettability of *h*-BN YSZ coating with molten volcanic ash, preliminary wetting experiments were performed under vacuum, for a duration of 1 hour. We find that the three volcanic ash samples evolved to form non-wetting, near-spherical molten droplets with high contact angles $\theta_c \sim 110^o$ when resting on the

h-BN YSZ, whereas they significantly wetted the surface of YSZ coating, evidenced by low contact angles θ_c ~ 40–55º (Figs. 4a and 4c; Movie S2). The results demonstrate that *h*-BN YSZ coating exhibit non-wettability to molten volcanic ash under vacuum.

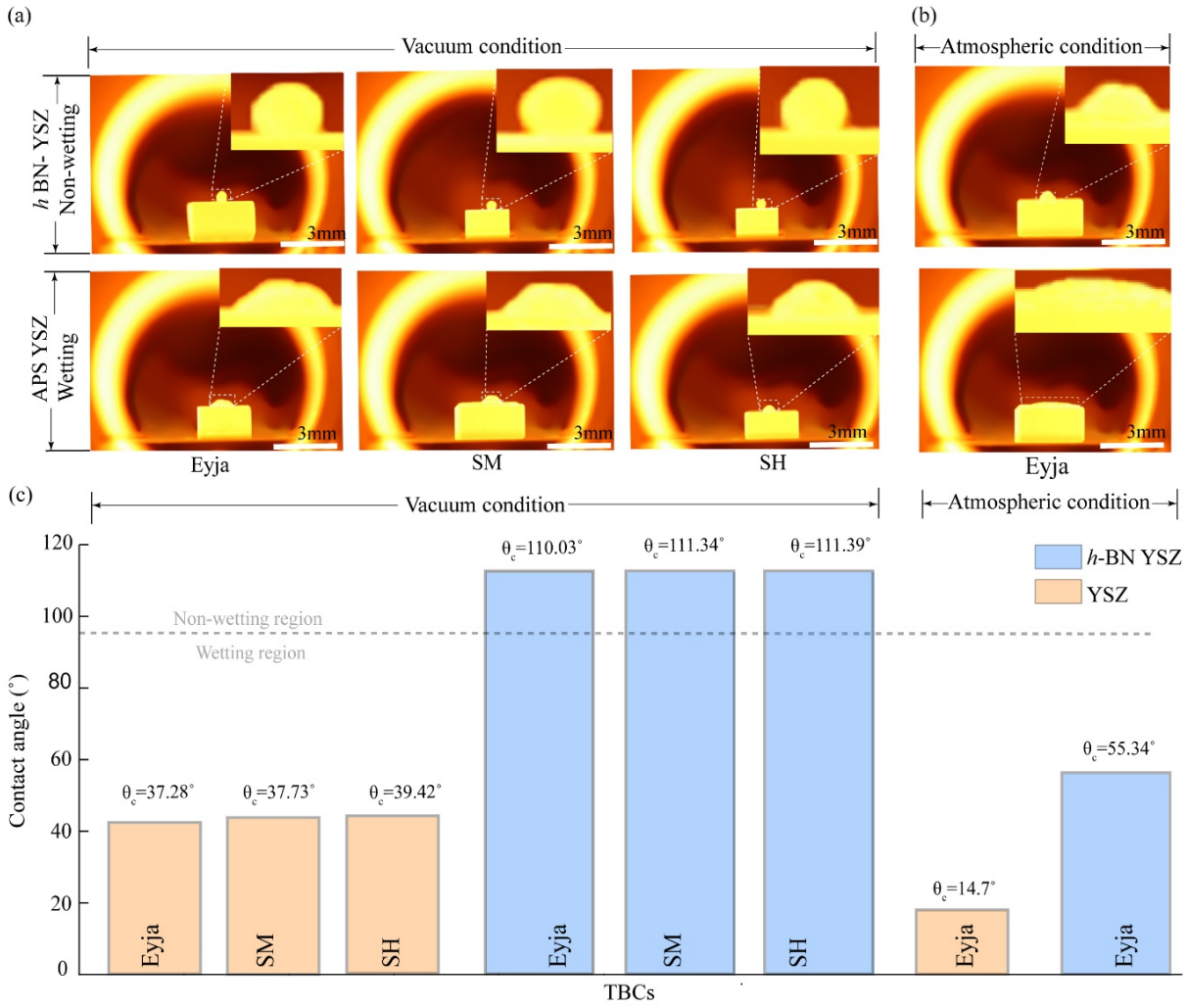

Fig. 4.Wettability of volcanic ash on conventional YSZ and novel *h*-BN YSZ coatings. (a) Photographs of the three volcanic ash droplets with variable wetting degrees on the surface of *h*-BN YSZ and YSZ coatings in-vacuo at 1250 °C. (b) Photographs of molten Eyja ash droplets on the *h*-BN YSZ and YSZ coatings at 1250 °C, in oxidizing condition. (c) Comparison of the contact angles resultant from the wetting of molten volcanic ash onto *h*-BN YSZ and conventional YSZ coatings in vacuum and atmospheric oxidizing conditions at 1250 °C.

Bearing in mind the potential oxidation of *h*-BN, we further determined the wetting properties of the coatings with Eyja ash under oxidizing atmospheric conditions. Eyja ash was chosen due to the lowest melting point and lowest viscosity at 1250 ºC compared with the other volcanic ash samples. Here, 1-hour hold-time tests were performed and *in-situ* images at 1250 ºC reveal that the melt completely spread onto the surface of YSZ coating (θ_c = 14.7º). Spreading of molten Eyja ash on *h*-BN YSZ (Figs. 4b and 4c) was

much more limited, exhibiting a contact angle $\theta_c = 55.34^o$, more than thrice that of conventional YSZ coating (Fig.4c and Movie S3). These results demonstrate that the novel *h*-BN YSZ coatings have an increased resilience to wetting by molten volcanic ash compared to YSZ coatings, under atmospheric conditions. In order to examine the influence of R_a on the wetting, *h*-BN YSZ of Ra= 3.43 ± 0.37 µm was fabricated (Fig. S3) and θ_c was found to be 51.5°, post wetting of molten Eyja ash for a soak-time of 1 hour (Movie S4). Thereby, it was inferred that the variation in R_a of *h*-BN YSZ coating did not influence the degree of wetting on the surface. To resolve the extent to which molten volcanic ash spreads onto the TBCs, the spreading area of the melt was evaluated. We note that the onset of colour fading was observed by the formation of a faint-brown ring/ corrosion ring (Fig. S4) [34]. The corrosion ring formed post 3 hrs for the YSZ coating, whereas it was observed post 12 hrs for the *h*-BN YSZ coating, that is 4 times longer. Surficial reaction as a result of complete wetting of the molten Eyja ash (θ_c~0), is evident from the formation of the corrosion ring, which is visible for a soak time of 3 hours on YSZ coating, in contrast to 12 hrs long term exposure of *h*-BN YSZ coatings.

3.3 Infiltration resistance of *h*-BN YSZ against molten volcanic ash

The infiltration of molten Eyja in the coatings after thermal aging was determined by the elemental distribution of Si, mapped across the cross-section of the coatings. θ_c made by molten Eyja on the surface of *h*-BN YSZ was 43°during a soak time of 3 hrs and 16°during a soak time of 6 hrs at 1250 °C (See Fig. S5), whereas molten Eyja thoroughly wetted the surface of YSZ coatings for a soak-time of 3 hrs at 1250 °C (See Fig. S6). θ_c of thermally soaked *h*-BN YSZ was higher than conventional YSZ, this was related to its minimal infiltration as seen in Fig 5a. Previous studies on the modifications of the microstructure of TBCs suggested that a minor difference in θ_c, had a significant impact on the infiltration depth of molten CMAS into TBCs [35]. For a soak-time of 12 hrs, the maximum infiltration depth of *h*-BN YSZ (86 µm) was twice the infiltration depth of 6hrs thermally aged *h*-BN YSZ (43 µm) (Figs. 5a and 5b). Previous research on Alumina doped YSZ has also documented shallow penetration of molten CMAS into a highly porous coating [36]. Here, we observe that the lower wetting propensity of molten ash on *h*-BN YSZ versus YSZ coating had a significant impact on the infiltration depth, presumably owing to the reactive wetting of *h*-BN and

molten silicate. The inter-relationship between thermal aging and variation in contact angle was observed as the molten volcanic ash completely wetted the surface of 12 hrs thermally aged *h*-BN YSZ coating from 16 ° of 6 hrs thermally aged *h*-BN YSZ coating. However, the lower sub-region of the 12 hrs thermally aged *h*-BN YSZ coating was unaffected by infiltration and the influence of oxidation could be minor (Fig. 5b), due to the presence of N in the underlying unaffected layer (See Fig. S7). It should be noted that the infiltration of molten volcanic ash results in the reduction of porosity of the coatings, and increases the thermal conductivity[37]. From Fig. 5c it is observed that the average porosity of 12-hrs thermally aged *h*-BN YSZ coating was 3.6 times higher than APS coating, this might be the reason for the minimal influence of oxidation to the underlying unaffected layer of *h*-BN YSZ coating. However, to conclude regarding the oxidation aspect of the novel coatings, an in-depth thermo-chemical analysis of *h*-BN YSZ and molten silicate interaction is required.

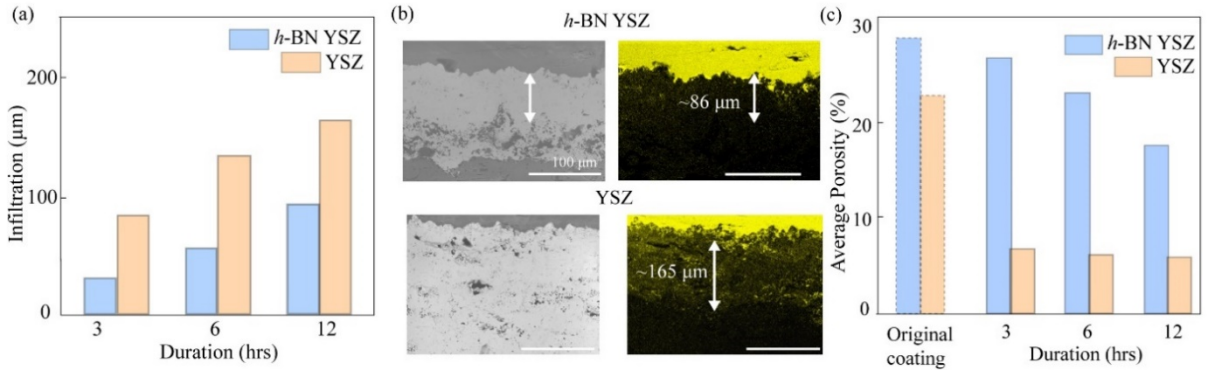

Fig. 5. Infiltration of molten of Eyja ash into the coatings at atmospheric condition. (a) Maximum infiltration depth (µm) of molten volcanic ash into each TBC. (b) Si-Elemental maps of *h*-BN YSZ and YSZ coating for soak-time of 12 hrs at 1250 °C. (c) Average porosity (%) of as-sprayed coatings and coatings infiltrated by molten volcanic ash.

The coatings were further subjected to thermal aging for 48 hours, and it was observed that there was no residual glass present on the surface of the coatings and molten Eyja completely reacted with the coatings (see Fig. S8). It was evident that the conventional YSZ coatings completely reacted with molten Eyja. Whereas *h*-BN YSZ coating was prone to the reaction in an uneven manner, with an increase in density of globular Si-based reaction products. The reason behind this phenomenon is still unclear and our future work will be directed to produce uniform layered *h*-BN YSZ coating structure, in order to investigate this behavior.

3.4 Mechanical properties

Micro-hardness values of the coatings subjected to infiltration by molten Eyja, for a soak time of three hours was evaluated. The average micro-hardness values of as-sprayed conventional YSZ (6.55 ± 1.2 GPa) and *h*-BN YSZ coatings (6.52 ± 0.5 GPa) were nearly the same. The micro-hardness of molten Eyja infiltrated coatings was measured across the cross-section, tracking the infiltration depths at 50, 75, 100 and 150 µm respectively. At an infiltration depth of 50 µm (example: Fig. 6a and 6b), it was evident that both conventional YSZ (9.23 ± 0.89 GPa) and *h*-BN YSZ (8.51 ± 0.72 GPa) coatings exhibited high micro-hardness values (Fig. 6c), due to the infiltration of molten Eyja. At 75 µm, conventional YSZ coating (9.06 ± 0.44 GPa) exhibited higher micro-hardness values than *h*-BN YSZ coating (6.76 ± 0.56 GPa), this corresponds to the presence of molten Eyja in conventional YSZ coating, as the micro-hardness value of solidified Eyja glass shard (Fig. S9) was measured to be 5.19 ± 0.6 GPa.

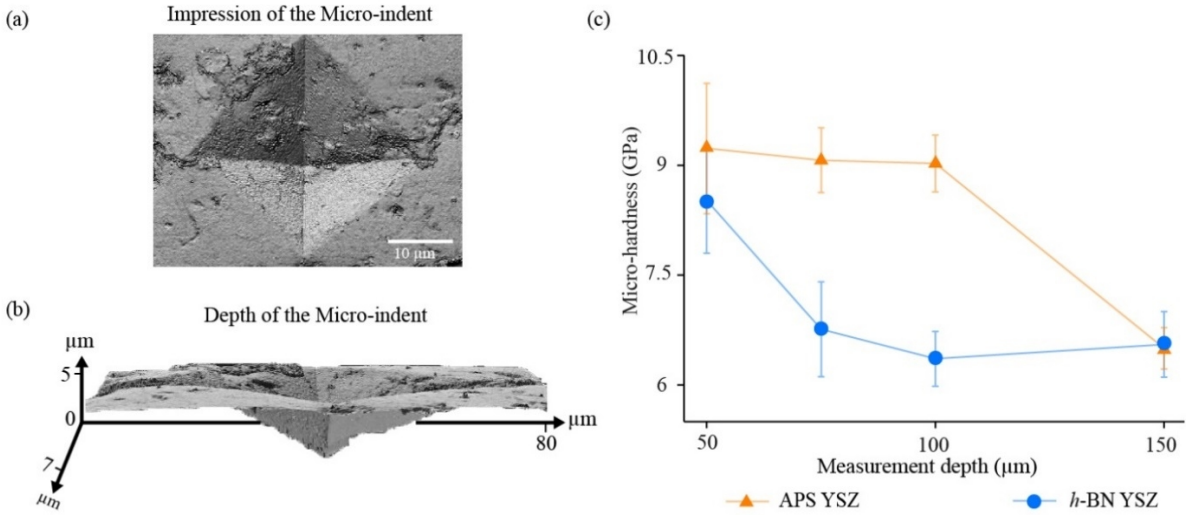

Fig. 6. Micro-hardness of the coatings. (a) Indent impression of h-BN YSZ coating. (b) Depth of indent impression on h-BN YSZ coating. (c) Change in the micro-hardness corresponding to the measurement depth

The infiltration of molten Eyja into the coating and further solidification led to the increase in micro-hardness value (accompanied by stiffening), which results in the mechanical degradation of the coating [38, 39]. *H*-BN YSZ coatings exhibit better stiffening resistance than the conventional YSZ coatings, as wetting of the coatings play a governing role in the infiltration of molten volcanic ash thereby influencing the micro-hardness value.

4. Conclusion

In order to counteract the propensity of ingested, molten volcanic ash droplets to wet and infiltrate TBCs and cause damage to jet engines, we have developed and tested new *h*-BN YSZ coatings which exhibit enhanced resistant behavior against molten volcanic ash wetting. Employing controlled laboratory testing, we first demonstrated that pure *h*-BN substrates have silica-phobic properties under vacuum conditions at 1250 °C. Further, we have fabricated novel coatings containing 80 wt.% YSZ and 20 wt.% *h*-BN, and tested their ability to resist molten volcanic ash droplets, compared to conventional YSZ coating. Under vacuum conditions, this new coating repelled volcanic ash droplets, preventing infiltration of the substrate, unlike the conventional coating. Under oxidizing conditions, *h*-BN YSZ coating appeared more resilient as we find that molten ash only partially wets the substrate *i.e.* the molten ash spread less and more slowly on *h*-BN YSZ *versus* conventional TBCs. *H*-BN YSZ coating exhibited better stiffening resistance than conventional YSZ coating, due to their resilience against rapid wetting and infiltration of molten volcanic ash. The thermo-mechanical aspect of degradation and potential challenges like the prevalence of water vapor in a gas-turbine environment on *h*-BN YSZ, will be discussed in the future. This work extends the scope for physicochemically resilient "silica-phobic" TBCs with *h*-BN additives, which possess the potential for mitigating risks associated with volcanic ash ingestion into jet engines. Further investigations employing such TBC solutions against other atmospheric contaminants, as well as testing of its performance under severe thermal cycling conditions are underway.

Data availability

The data supporting the findings of this study are available from the corresponding author upon reasonable request.

Acknowledgements

We are grateful to Nakanishi Hironobu from Toyohashi University of Technology for supporting this research in the use of thermal spray technology, Corrado Cimarelli for providing the sample material and assistance in SEM measurements. W. Song acknowledges the support of "Freigeist" Fellowship of the Volkswagen Stiftung on "Volcanic Ash Deposition in Jet Engines" (VADJEs, No 89705).

References

[1] W.S. Smith, High-altitude conk out, Natural History Mag. 92 (1983) 26–34.

[2] A.J. Prata, I.J. Barton, R.W. Johnson, K. Kamo, J. Kingwell, Hazard from volcanic ash, Nature 354 (1991) 25. Doi: 10.1038/354025a0.

[3] T.J. Casadevall, Volcanic hazards and aviation safety-lessons of the past decade, FAA Aviation Safety J. 2 (1992) 9–17.

[4] F. Prata, I. Barton, J. Kingwell, Aircraft hazard from volcanoes, Nature 366 (1993) 199. Doi: 10.1038/366199a0.

[5] Z.J. Przedpelski, T. Casadevall, Impact of volcanic ash from 15 December 1989 Redoubt volcano eruption on GE CF6-80C2 turbofan engines, U.S. Geol.Survey Bull. 2047 (1994) 129–135.

[6] P. Brooker, Fear in a handful of dust: aviation and the icelandic volcano, Significance 7 (2010) 112–115. Doi: 10.1111/j.1740-9713.2010.00436.x.

[7] G. Li, C. Cai, Y. Wang, Y. Zhou, L. Yang, J. Lu, G. Zhou, Zirconium silicate growth induced by the thermochemical interaction of yttria-stablized zirconia coatings with molten CMAS deposits, Corros. Sci. 149 (2019) 249–256. Doi: 10.1016/j.corsci.2019.01.011.

[8] T. Bolić, Ž. Sivčev, Eruption of Eyjafjallajökull in Iceland: Experience of European air traffic management, Transp.Res. Rec. J. Transp. Res. Board 2214 (2011)136–143. Doi: 10.3141/2214-17.

[9] S.R. Gislason, H. A. Alfredsson, E.S. Eiriksdottir, T. Hassenkam, S.L.S. Stipp, Volcanic ash from the 2010 Eyjafjallajökull eruption, Appl. Geochemistry 26 (2011) S188–S190. Doi: 10.1016/j.apgeochem.2011.03.100.

[10] W. Song, K. Hess, D.E. Damby, F.B. Wadsworth, Y. Lavallée, C. Cimarelli, D.B Dingwell, Fusion characteristics of volcanic ash relevant to aviation hazards. Fusion characteristics of volcanic ash relevant to aviation hazards, Geophys. Res. Lett. 41 (2014) 2326–2333.

[11] W. Song, Y. Lavallée, F.B. Wadsworth, K.-U. Hess, D.B. Dingwell, Wetting and Spreading of Molten Volcanic Ash in Jet Engines, J. Phys. Chem. Lett. 8 (2017) 1878–1884. doi:10.1021/acs.jpclett.7b00417.

[12] J.H. Perepezko, The hotter the engine, the better, Science 326 (2009) 1068–1069. Doi: 10.1126/science.1179327.

[13] S. Kraemer, J. Yang, C.G. Levi, C.A. Johnson, Thermomechanical interaction of thermal barrier coatings with molten CaO-MgO-Al_2O_3-SiO_2 (CMAS) Deposits, J. Am. Ceram. Soc. 89 (2006) 3167–3175. Doi: 10.1111/j.1551-2916.2006.01209.x.

[14] W. Song, Y. Lavallée, K.U. Hess, U. Kueppers, C. Cimarelli, D.B. Dingwell, Volcanic ash melting under conditions relevant to ash turbine interactions, Nat.Commun. 7 (2016) 10795. Doi: doi.org/10.1038/ncomms10795.

[15] N.P. Padture, M. Gell, E.H. Jordan, Thermal barrier coatings for gas-turbine engine applications, Science 296 (2002) 280–284. Doi: 10.1126/science.1068609.

[16] D.R. Clarke, M. Oechsner, N.P. Padture, Thermal-barrier coatings for more efficient gas turbine engines, MRS Bull. 37 (2012) 891–897. Doi: 10.1557/mrs.2012.232.

[17] N.P. Padture, Advanced structural ceramics in aerospace propulsion, Nat. Mater. 15 (2016) 804–809. Doi: 10.1038/nmat4687.

[18] W. Song, S. Yang, M. Fukumoto, Y. Lavallée, S. Lokachari, H. Guo, Y. You, D.B. Dingwell, Impact interaction of in-flight high-energy molten volcanic ash droplets with jet engines, Acta Mater. 171 (2019) 119–131. Doi: 10.1016/j.actamat.2019.04.011.

[19] X.Q. Cao, R. Vassen, D. Stoever, Ceramic materials for thermal barrier coatings, J. Eur.Ceram. Soc. 24 (2004) 1–10. Doi: 10.1016/S0955-2219(03)00129-8.

[20] S. Sampath, U. Schulz, O.M. Jarligo, S. Kuroda, Processing science of advanced thermal-barrier systems, MRS Bull. 37 (2012) 903–910. Doi: 10.1557/mrs.2012.233.

[21] X. Zhou, T. Chen, J. Yuan, Z. Deng, H. Zhang, J. Jiang, X. Cao, Failure of plasma sprayed nano-zirconia-based thermal barrier coatings exposed to molten CaO–MgO–Al_2O_3–SiO_2 deposits, J. Am. Ceram. Soc. 102 (2019) 6357–6371. Doi:10.1111/jace.16498.

[22] X. Zhou, B. Zou, L. He, Z. Xu, J. Xu, R. Mu, X. Cao, Hot corrosion behaviour of $La_2(Zr_{0.7}Ce_{0.3})_2O_7$ thermal barrier coating ceramics exposed to molten calcium magnesium aluminosilicate at different temperatures, Corros. Sci. 100 (2015) 566–578. Doi:https:10.1016/j.corsci.2015.08.031.

[23] J.M. Drexler, A.D. Gledhill, K. Shinoda, A.L. Vasiliev, K.M. Reddy, S. Sampath, N.P. Padture, Jet engine coatings for resisting volcanic ash damage, Adv. Mater. 23 (2011) 2419–2424. Doi: 10.1002/adma.201004783.

[24] J. Xia, L. Yang, R.T. Wu, Y.C. Zhou, L. Zhang, B.B. Yin ,Y.G. Wei, On the resistance of rare earth oxide-doped YSZ to high temperature volcanic ash attack, Surf. Coatings Technol. 307, (2016) 534–541. Doi: 10.1016/j.surfcoat.2016.09.033

[25] S. Krämer, J. Yang, C.G. Levi, Infiltration-inhibiting reaction of gadolinium zirconate thermal barrier coatings with CMAS melts, J. Am. Ceram. Soc. 91, (2008) 576–583. Doi: 10.1111/j.1551-2916.2007.02175.x.

[26] D. Giordano, J. Russell, D.B. Dingwell, Viscosity of magmatic liquids: a model, Earth Planet Sci. Lett. 271 (2008) 123–134. Doi:10.1016/j.epsl.2008.03.038.

[27] G.A.R. Gualda, M.S. Ghiorso, R.V. Lemons, T.L. Carley, Rhyolite-MELTS: A modified calibration of MELTS optimized for silica-rich, fluid-bearing magmatic systems, J Petrol. 53 (2012) 875–890. Doi: 10.1093/petrology/egr080.

[28] A. Stalder, G. Kulik, D. Sage, L. Barbieri, P. Hoffmann, A snake-based approach to accurate determination of both contact points and contact angles, Colloids Surf. A Physicochem. Eng. Asp. 286 (2006) 92–103. Doi: 10.1016/j.colsurfa.2006.03.008.

[29] Z. Liu, Y. Gong, W. Zhou, L. Ma, J. Yu, J.C. Idrobo, J. Jung, A.H. MacDonald, R. Vajtai, J. Lou, P. M. Ajayan, Ultrathin high-temperature oxidation-resistant coatings of hexagonal boron nitride, Nat. Commun. 4 (2013) 2541. Doi: 10.1038/ncomms3541.

[30] E. Wuchina, E. Opila, M. Opeka, W. Fahrenholtz, I.G. Talmy, UHTCs: Ultra-high temperature ceramic materials for extreme environment applications, Electrochem. Soc. Interface 16 (2007) 30–36. ISSN: 1064–8208.

[31] B. Drevet, R. Voytovych, R. Israel, N. Eustathopoulos, wetting and adhesion of Si on Si_3N_4 and BN substrates, J. Eur. Ceram. Soc. 29 (2009) 2363–2367. Doi: 10.1016/j.jeurceramsoc.2009.01.024.

[32] W. Polkowski, N. Sobczak, R. Nowak, A. Kudyba, G. Bruzda, A. Polkowska, M. Homa, P. Turalska, M. Tangstad, J. Safarian, E. Moosavi-Khoonsari, A. Datas, Wetting behavior and reactivity of molten silicon with h-BN substrate at ultrahigh temperatures up to 1750 °C, J. Mater. Eng. Perform. 27 (2018) 5040–5053. Doi: 10.1007/s11665-017-3114-8.

[33] Z. Yuan, W.L. Huang, K. Mukai, Wettability and reactivity of molten silicon with various substrates, Appl. Phys. A. 78 (2004) 617–622. Doi: 10.1007/s00339-002-2001-8.

[34] N. Eustathopoulos, Progress in understanding and modeling reactive wetting of metals on ceramics, Curr. Opin. Solid State Mater. Sci. 9 (2005) 152–160. Doi: 10.1016/j.cossms.2006.04.004.

[35] R. Naraparaju, J.J. Gomez Chavez, P. Niemeyer, K.U. Hess, W. Song, D.B. Dingwell, S. Lokachari, C. V Ramana, U. Schulz, Estimation of CMAS infiltration depth in EB-PVD TBCs: A new constraint model supported with experimental approach, J. Eur. Ceram. Soc. (2019). Doi: 10.1016/j.jeurceramsoc.2019.02.040.

[36] B. Yin, F. Zhang, W. Zhu, L. Yang, Y. Zhou, Effect of Al_2O_3 modification on the properties of YSZ: Corrosion resistant, wetting and thermal-mechanical properties, Surf. Coatings Technol. 357 (2019) 161–171. Doi: 10.1016/j.surfcoat.2018.09.048.

[37] J. Wu, H. bo Guo, Y. zhi Gao, S. kai Gong, Microstructure and thermo-physical properties of yttria stabilized zirconia coatings with CMAS deposits, J. Eur. Ceram. Soc. 31 (2011) 1881–1888. doi:10.1016/j.jeurceramsoc.2011.04.006.

[38] Y. Hayashi, S. Lokachari, S. Yamagishi, M. Okazaki, Material and mechanical aspects of CMAS damage progression on thermal barrier coatings and its non-destructive detection, 2017. Doi: 10.4028/www.scientific.net/MSF.879.720.

[39] S. Lokachari, W. Song, J. Yuan, M. Kaliwoda, D.B. Dingwell, Influence of molten volcanic ash infiltration on the friability of APS thermal barrier coatings, Ceram. Int. (2020). Doi: 10.1016/j.ceramint.2020.01.166.

Novel Thermal Barrier Coatings with Hexagonal Boron Nitride Additives Resistant to Molten Volcanic Ash Wetting

Siddharth Lokachari [a], Wenjia Song [a,*], Masahiro Fukumoto [c], Yan Lavallée [d], Hongbo Guo [e], Yancheng You [b,*], Donald B. Dingwell [a]

[a] Department of Earth and Environmental Sciences, Ludwig Maximilians Universität München, Theresienstrasse 41, 80333 Munich, Germany

[b] School of Aerospace Engineering, Xiamen University, 361102 Xiamen, China

[c] Department of Mechanical Engineering, Toyohashi University of Technology, 1-1 Tempaku-cho, 441-8580 Toyohashi, Japan

[d] Department of Earth, Ocean and Ecological Sciences, University of Liverpool, Liverpool L69 3GP, UK

[e] School of Materials Science and Engineering, Beihang University, 100191 Beijing, China

***Corresponding authors**:

Wenjia Song, Department of Earth and Environmental Sciences, Ludwig-Maximilians-Universität (LMU), Theresienstrasse 41, 80333 Munich, Germany. (wenjia.song@lmu.de)
Telephone: +49 (0) 89 2180 4293

Yancheng You, School of Aerospace Engineering, Xiamen University, 361102 Xiamen, China. (yancheng.you@xmu.edu.cn)

Telephone: +86 (0) 592 2186 849

Supporting Information

Movie Descriptions

Movie S1. Morphological silhouette transition of Eyja glass shard on *h*-BN substrate from room temperature to 1250 °C, performed in vacuum conditions.

Movie S2. Silhouette transition of Eyja, SM and SH ash pellets on conventional YSZ and h-BN YSZ coatings from room temperature to 1250 °C, performed in vacuum conditions.

Movie S3. Silhouette transition of Eyja ash pellet on conventional YSZ and h-BN YSZ coatings from room temperature to 1250 °C, performed in oxidizing conditions.

Movie S4. Influence of *h*-BN YSZ surface roughness on wetting of Eyja ash on the coating surface.

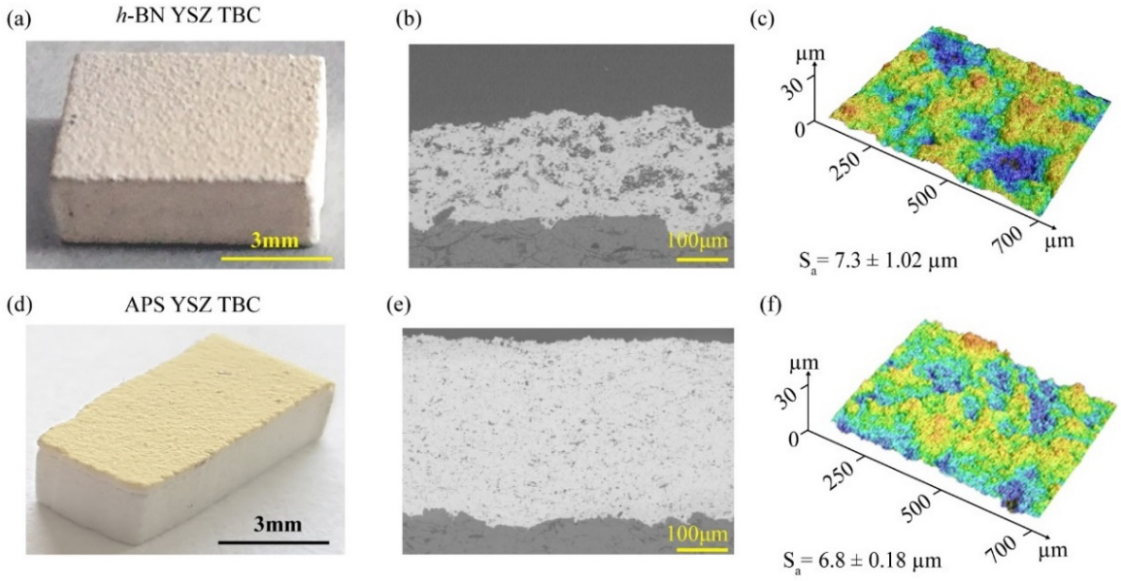

Fig. **S1**. Properties of *h*-BN YSZ and conventional APS YSZ coatings. (a) Photograph of *h*-BNYSZ coating (6 × 3 mm) fabricated by thermal spay deposition on an alumina substrate. (b) Cross-sectional SEM image of *h*-BN YSZ coating (thickness: ~ 200μm). (c) Surface roughness profile of *h*-BN YSZ coating topography evaluated by confocal laser microscopy. (d) Photograph of conventional APS YSZ coating (6 × 3 mm) on an alumina substrate. (e) Cross-sectional SEM image of APS YSZ coating (thickness: ~ 400μm) (f) Surface roughness profile of APS YSZ coating topography evaluated by confocal laser microscopy.

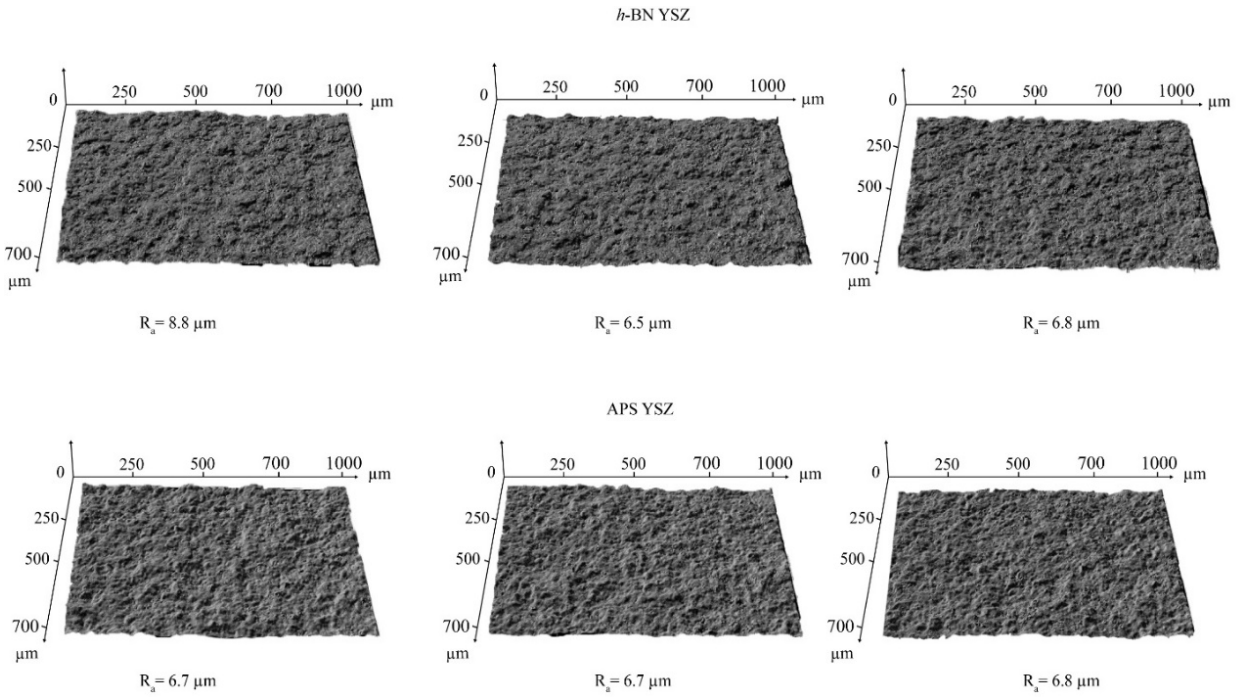

Fig. **S2**. Surface profile across *h*-BN YSZ and APS YSZ coatings.

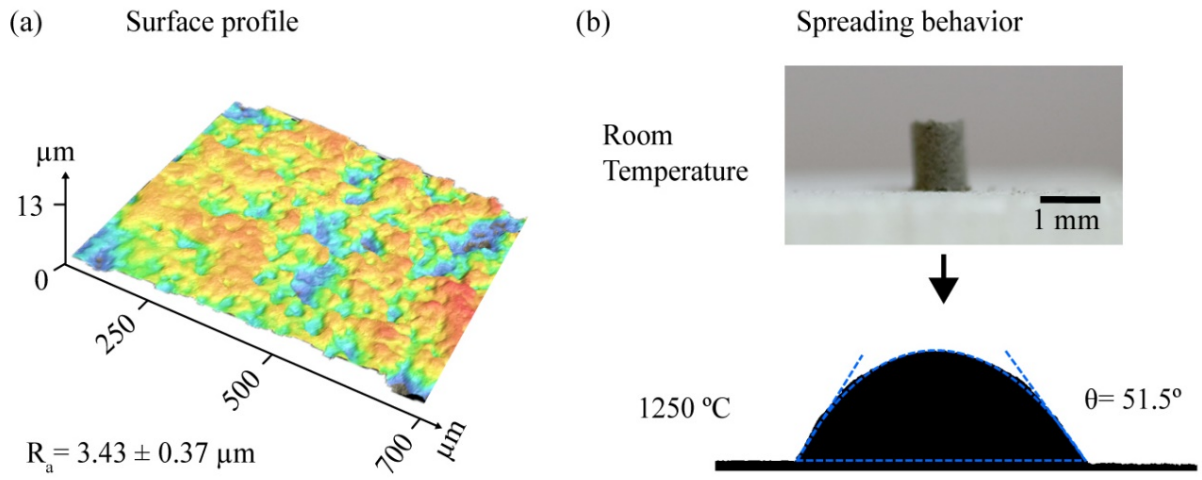

Fig. **S3**. Influence of R_a on wetting (a) R_a value of h-BN YSZ (b) spreading behavior.

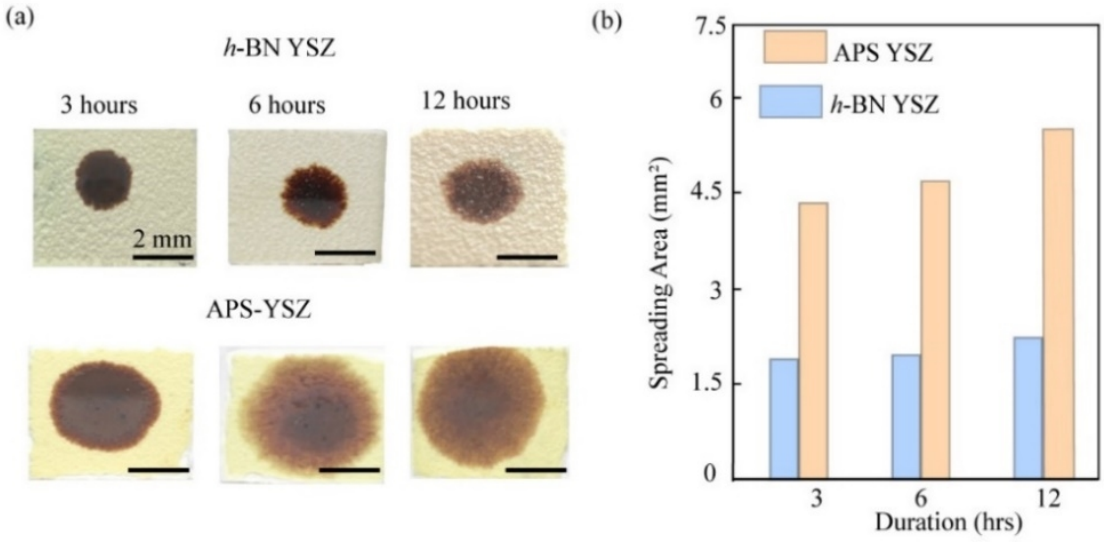

Fig. **S4**. Extent of Spreading of Eyja ash on the coatings under atmospheric condition. (a) Spreading of molten ash on the surface of h-BN YSZ (upper row) and conventional APS TBCs (lower row) at 1250 °C. (b) Comparison of the extent of spreading on the coatings.

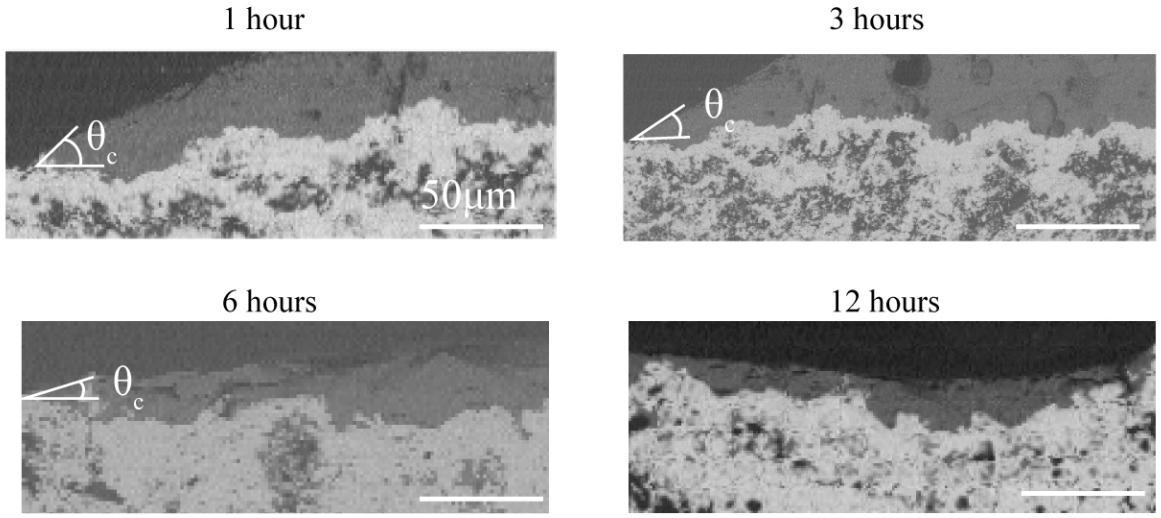

Fig. **S5**. Contact angle of molten Eyja ash on *h*-BN YSZ post thermal soak time of 1, 3, 6 and 12 hours.

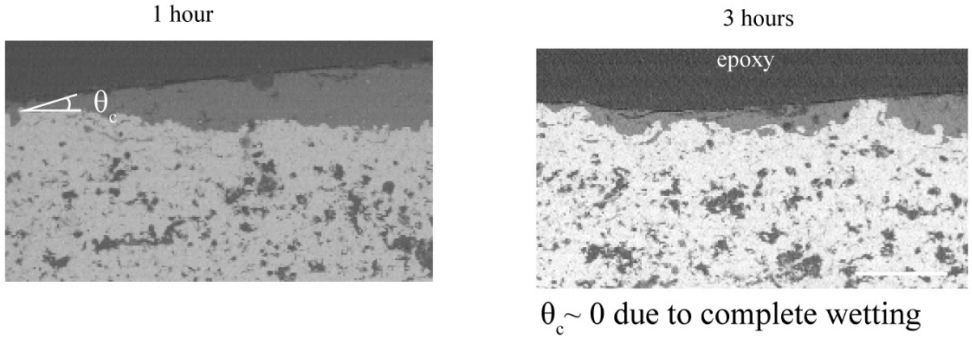

Fig. **S6**. Contact angle of molten Eyja ash on *h*-BN YSZ post thermal soak time of 1 and 3 hours

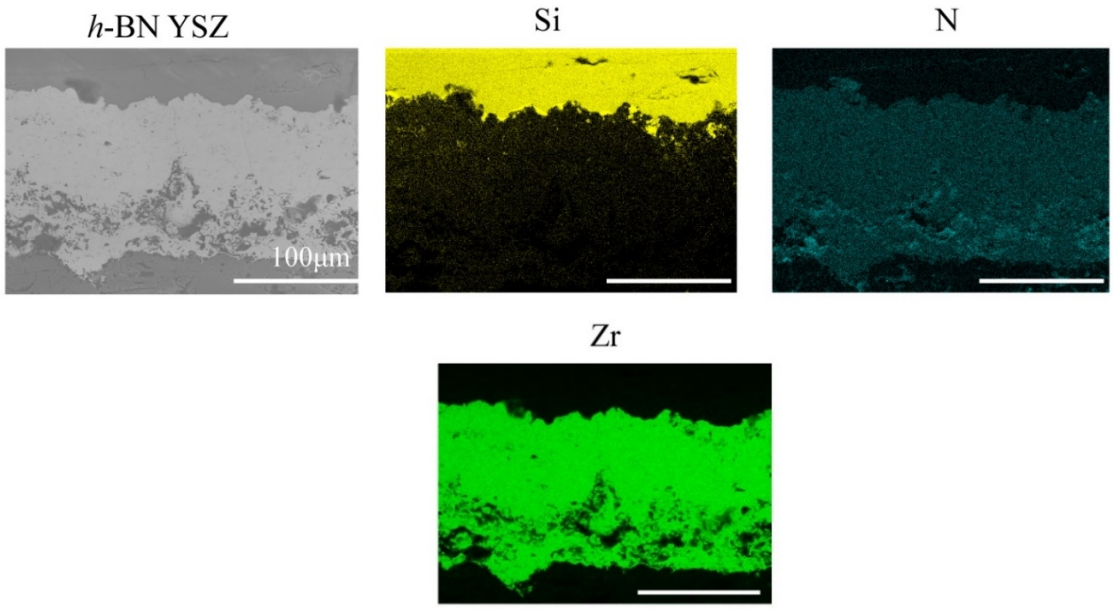

Fig. **S7**. EDS elemental maps of 12hrs thermally soaked *h*-BN YSZ coating.

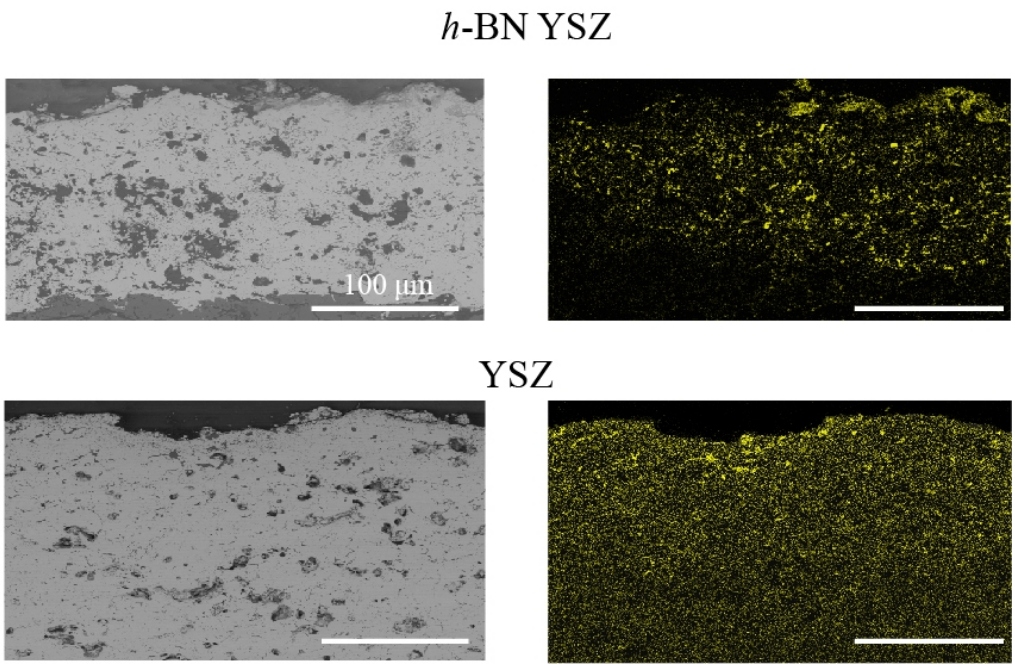

Fig. **S8**. Si elemental maps of 48hrs thermally soaked *h*-BN YSZ and conventional YSZ coatings.

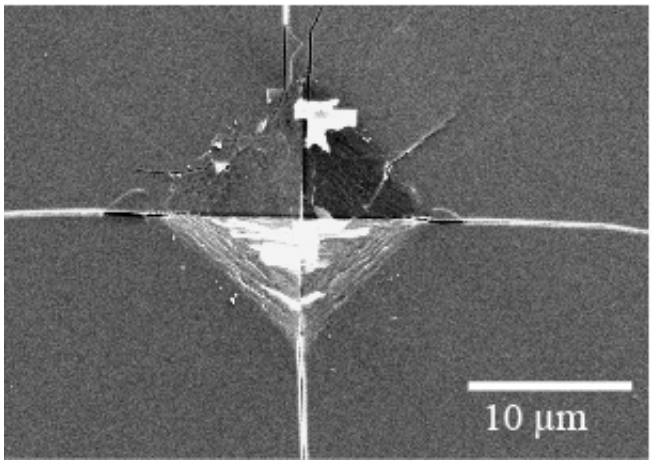

Fig. **S9**. Impression of the indent on the Eyja glass shard.

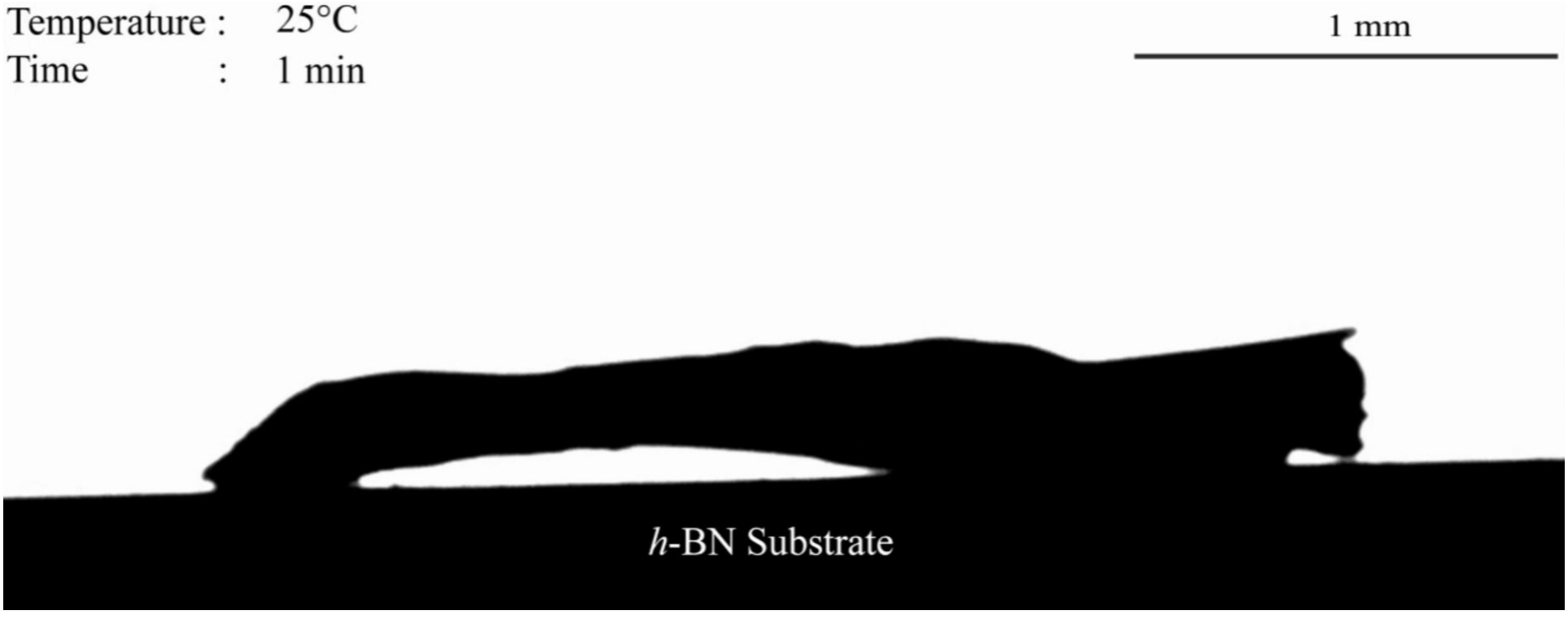
Temperature : 25°C
Time : 1 min
1 mm
h-BN Substrate

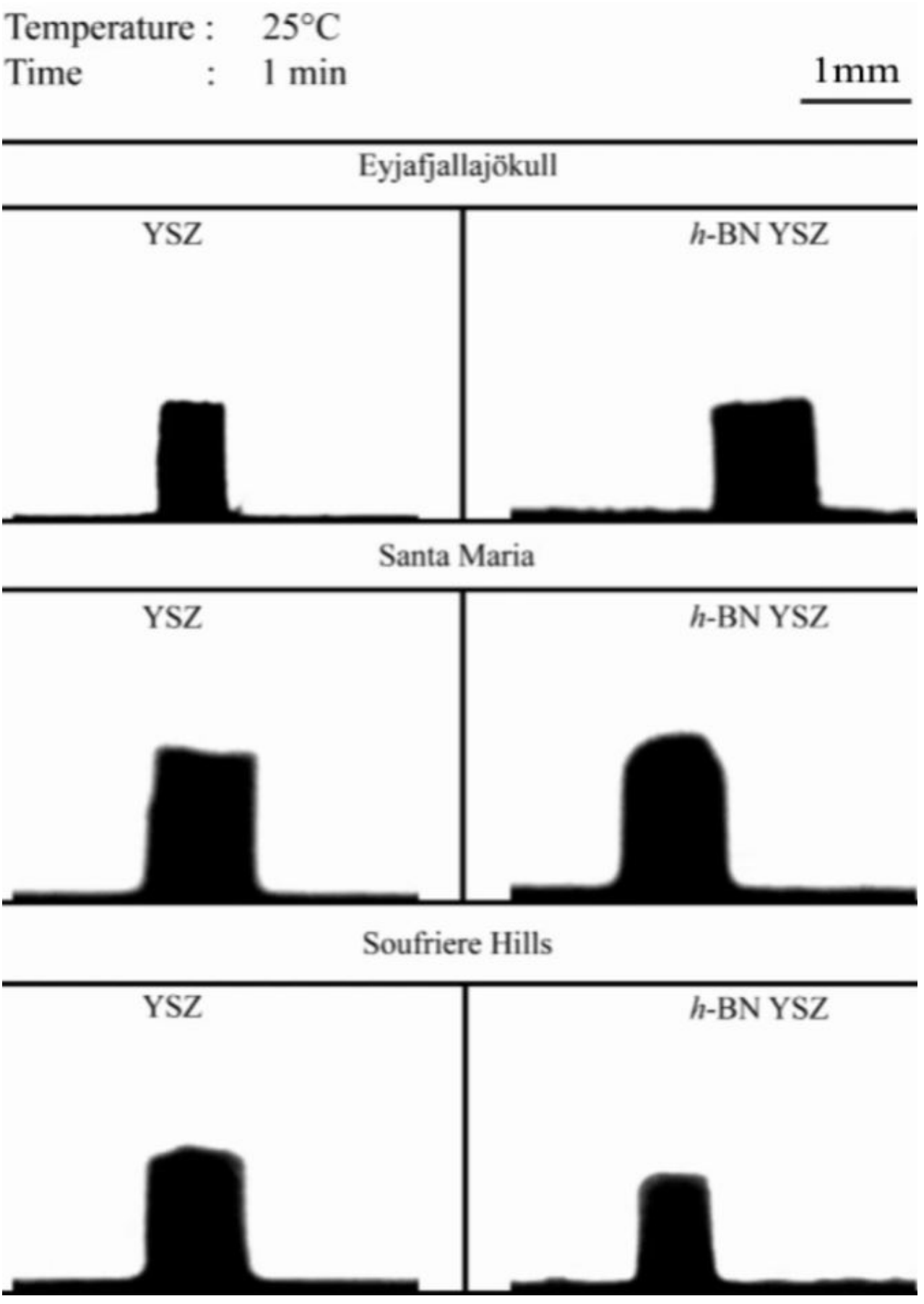
Temperature : 25°C
Time : 1 min
1mm
Eyjafjallajökull
YSZ
h-BN YSZ
Santa Maria
YSZ
h-BN YSZ
Soufriere Hills
YSZ
h-BN YSZ

Temperature : 25°C
Time : 1 min
Volcanic ash : Eyjafjallajökull

1 mm

YSZ

h-BN YSZ

h-BN YSZ

Temperature : 25°C

Time : 1 min

Volcanic ash : Eyjafjallajökull